Development of bulk quasicrystalline materials by spray forming

V.C.Srivastava[1*], E. Huttunen-Saarivirta[2], C. Cui[3], V. Uhlenwinkel[3], A.Schulz[3], N.K. Mukhopadhyay[4]

[1]National Metallurgical Laboratory, Jamshedpur-831007, India
[2]Department of Materials Science, Tampere University of Technology, P.O. Box 589, Tampere FIN-33101, Finland
[3]Institut für Werkstofftechnik, Universität Bremen, Badgasteiner Strasse 3, 28359 Bremen, Germany
[4]Department of Metallurgical Engineering, Indian Institute of Technology (BHU) Varanasi-221005, India
*Corresponding author: V.C.Srivastava (vcsrivas@nmlindia.org)

Abstract

In this study, Al-Cu-Fe based stable quasicrystalline alloys were spray deposited in bulk (around 40 kg), with and without addition of Sn. The spray deposited materials were characterized in terms of microstructure, hardness and thermal stability. The results showed that the $Al_{62.5}Cu_{25}Fe_{12.5}$ alloy contains the single quasicrystalline icosahedral phase (i-phase) along with a minor λ-$Al_{13}Fe_4$ phase, whereas the $Al_{62.5}Cu_{25}Fe_{12.5}$+Sn alloy contains five phases: the major i-phase, β-Sn, θ-Al_2Cu, λ-$Al_{13}Fe_4$ and β-AlFe(Cu) phases. These results have been corroborated by X-ray diffraction (XRD), scanning and transmission electron microscopy (SEM and TEM) and differential scanning calorimetry (DSC). The hardness value of the Al-Cu-Fe alloy reached 10.5 GPa at 50 g load, while that for Al-Cu-Fe-Sn alloy was somewhat lower. DSC analysis showed only one transformation peak at 885.5 ^{o}C for i-phase in $Al_{62.5}Cu_{25}Fe_{12.5}$, indicating the melting temperature. The present study provides an insight into the mechanism of phase and microstructural evolutions during spray forming of the studied alloys. The role of Sn in terms of microstructure and properties is highlighted.

Keywords: Quasicrystalline; icosahedral Phase; Al-Cu-Fe alloy; Tin; Spray forming

1.0 Introduction

Quasicrystalline materials are characterized as aperiodically long-range ordered solids which give rise to several distinctive properties, such as high hardness, low thermal conductivity, high corrosion and oxidation resistance and low coefficient of friction [Hut04]. These properties make them useful for several technological applications. Quasicrystalline Al-Cu-Fe alloys are found to be attractive for the bulk synthesis due to the wide availability of its constituent elements [Nic08]. Al-Cu-Fe system in the composition range of 58-70 at.% Al, 20-28 at.% Cu and 10-14 at.% Fe, containing stable icosahedral quasicrystalline (QC) phases, have been extensively studied [Hut04, Lee01, Hut05, Bar01, Nic08, Tur07, Yin07, Yin08, Li00, Sor95]. In general, the processing routes for such materials are restricted to melt spinning [Hut05], melt atomization [Li00, Sor95], mechanical alloying [Bar01, Eck91, Nic08, Tur07, Yin07, Yin08] and plasma spraying [Fle00], which typically produce QC powder or thin coatings. Further, a conventional casting route [Lee01, Fle04, Ros07] has also been employed, but with little success in obtaining a single-phase QC material. In general, residues of a crystalline

β-AlFe(Cu) phase co-exist with the QC phase, due to an incomplete peritectic reaction. A recent study by Nicula et al. [Nic08] demonstrated the formation of a bulk single-phase nano-quasicrystalline material by pulsed current sintering of mechanically alloyed nano-powders containing the β-Al(Cu,Fe) and θ-Al$_2$Cu phases. Similarly, Turquier et al. [Tur07] reported the possibility of obtaining a single-phase QC material by mechanical alloying and a following heat treatment. Overall, it is obvious that a number of studies have been carried out to produce single-phase quasicrystalline materials, many of which involve powder processes or otherwise require several process steps.

In their work, Srivastava et al. [Sri08] have showed the formation of bulk single-phase Al-Cu-Fe based quasicrystalline alloy in a single step using spray forming process. This process seems to be an attractive means of introducing single-phase QC alloys materials. In addition to the described overall challenges in processing QC materials, another feature which restricts the possible application of QC alloys as structural materials is their inherent brittleness. Recently, this limitation has been overcome to some extent by incorporation of soft and ductile phases into the quasicrystalline matrix, to improve toughness of the quasicrystalline materials [Fle04, Sha04, Sor98, Bis05]. Besides the spray-forming process employed to synthesise QC Al-Cu-Fe alloy, another unique feature of this paper is that this process is also used to produce Al-Cu-Fe alloy which contains a QC phase and a soft Sn-containing phase, to provide less brittle material.

Hence, in the present investigation, the well-established spray forming process [Gra95, Sri04, Pry02] is utilized to synthesize a single-phase Al-Cu-Fe based alloy with and without the addition of a soft Sn-containing phase. The study reports microstructures of the two different alloys and attempts to understand the mechanism of microstructural evolution during spray forming of large-size billets. These two themes are discussed in light of the inherent rapid solidification effect in spray forming and the solidification conditions of the droplets in the spray and the solidification of the deposit. The role of Sn alloying is also presented and discussed.

2.0 Experimental details

2.1. Materials

The materials selected for spray forming were of the nominal compositions of Al$_{62.5}$Cu$_{25}$Fe$_{12.5}$ and Al$_{62.5}$Cu$_{25}$Fe$_{12.5}$ + 10 wt.%Sn. Total amounts of 58 kg and 64 kg were used for spray forming of Al-Cu-Fe and Al-Cu-Fe+Sn alloys, respectively. Commercial purity elements (with a purity of 99.9%) were used for melting in an alumina crucible using an induction furnace.

2.2 Spray Forming

The spray forming experiments were carried out at the spray forming plant (SK-2) at the University of Bremen, Germany. A schematic of the spray forming set up is shown in Fig. 1. It consisted of a crucible, a tundish, an atomizer and a substrate. The required amount of elemental materials were melted together in the crucible under the nitrogen gas atmosphere, homogenized for 15 min and then poured into the tundish. The liquid stream was disintegrated into a spray of droplets using high velocity nitrogen gas employing a free-fall nozzle assembly. The spray of droplets was collected onto an inclined rotating steel substrate to give rise to a billet with 200 mm diameter and 350 mm height. The deposition distance, the scan angle, the spray scan frequency, substrate rotation frequency and deposit withdrawal rate were kept constant in both the experiments at 430 mm, ± 4°, 15.2 Hz, 2 Hz and 1 mm/s, respec-

tively. Both the alloys were poured into tundish at a temperature of about 1170 $^{\circ}$C. A yield of around 70% was achieved in both the experiments. Large size billets were successfully deposited although a number of macro-cracks were formed at the billet surface during cooling, leading to the fracture of the billets.
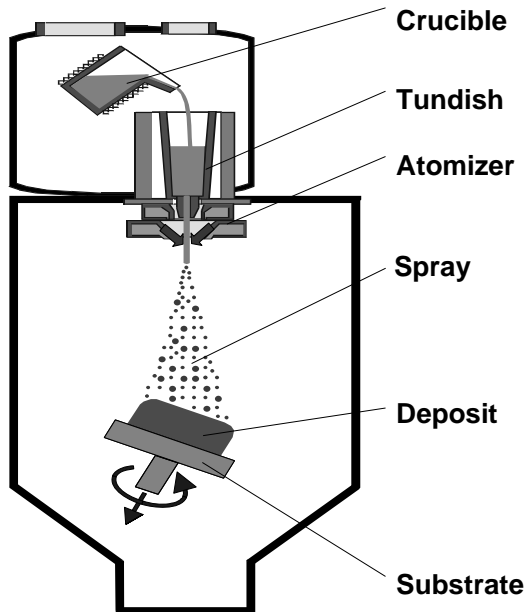
Crucible

Tundish

Atomizer

Spray

Fig. 1: A schematic of the spray forming system (SK-2) at the Institute fuer Werkstofftechnik, University of Bremen, Germany

Deposit

Substrate

2.3 Materials Characterization

Optical and scanning electron microscopy were carried out on spray-deposited materials, after using standard metallographic technique of sample preparation. A diluted Keller's reagent (194 ml H_2O, 3 ml HNO_3, 2 ml HF and 1 ml HCl) was used as etchant for both the alloy compositions. The X-ray element maps and EDX point analyses were performed for both the alloys to have the idea of different phases and element distribution in the spray-deposited materials. The deposits and the sieved overspray powders were analyzed by X-ray diffraction using Cu-K$_{\alpha}$ radiation. The microstructural characterization was carried out by optical microscope (Leica DM2500) and Scanning electron microscope ((SEM Gemini 1530).

The Al-Cu-Fe alloys were further examined by transmission electron microscope JEM 2010 (Jeol, Japan), at an accelerating voltage of 200 kV. The transmission electron microscopy studies were performed for powder samples that were prepared from the sections of fractured spray-deposited Al-Cu-Fe billet by carefully crushing in a mortar.

In addition to microstructural characterisation, thermal analysis was performed for both the alloys to study their phase constitution and stability of the phases using a simultaneous thermal analyser STA 409 by Netzsch (Germany). Measurements were carried out using a high-temperature differential scanning calorimetry (DSC) sample carrier and Al_2O_3 sample pans under an argon flow of 50 ml min^{-1} at a heating rate of 5°C min^{-1} through the temperature range of 20-1400°C. The phase transformations were identified using the data analysis program, by determining the start and finish temperatures of phase transformation. These were then compared to values reported in the literature. The samples were heat treated at different temperatures to see the transformation and stability of phases.

Vickers hardness measurements were carried out at different indentation loads and the crack length starting from the corners of the indentation was measured. The indentations were observed under optical as well as scanning electron microscope to see the variation in behaviour of indentation cracks in both the alloys. The hardness data shown is an average of at least 5 measurements.

3. Results

3.1 Microscopy

Optical microscopy

The optical micrographs of the spray deposited Al-Cu-Fe alloy are shown in Fig. 2. Fig. 2a shows the representative micrograph of the deposit, revealing a fine equiaxed grain structure with an average grain size of about 6 μm. However, there is evidently some variation in the grain size. The small black regions in the micrographs are pores. In addition to these fine-grained regions that form majority of the structure, some areas with larger grain size, about 70-80 μm, could also be detected (Fig. 2b). Moreover, small precipitates, in black contrast, were evident in the centre of larger grains; by composition, these were the $Al_{13}Fe_4$ phase, the topic which is discussed later. Figs. 2c and 2d represent the high magnification micrographs of the above two regions. Fig. 2c shows areas containing fine equiaxed grains and proves the observed variation in grain size, whereas, Fig. 2d reveals larger grains with embedded $Al_{13}Fe_4$ phase. It is interesting to note that the large grains showed evidence of twinning, in contrast to small equiaxed grains (Fig. 2d). The areas containing coarse grains also contained large pores at the grain boundaries, as indicated by arrows, in contrast to regions with smaller grain size. Furthermore, the fine-grained areas had spherical gas pores, whereas the coarse regions contained essentially interstitial or shrinkage pores. Figs. 2e and 2f show the micrographs of the materials obtained after holding at 840 ^{o}C for 1h in air. Fig. 2e indicates grain growth, withthe average grain size of about 12 μm. In contrast, the regions containing coarse grains disclosed the dissolution of the $Al_{13}Fe_4$ phase and the increase in the porosity level at the grain boundaries (Fig. 2f).
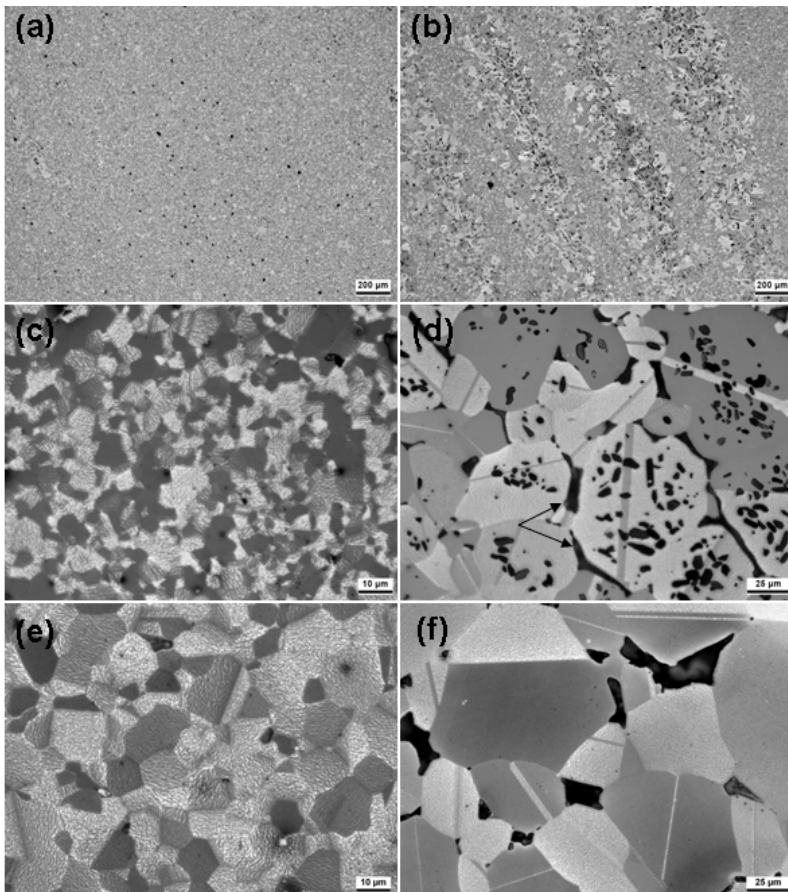

Fig. 2: Optical micrographs of the spray formed $Al_{62.5}Cu_{25}Fe_{12.5}$ (a) fine grain region (b) a layered structure of coarse and fine grains (c) high magnification micrographs of fine grained regions (d) high magnification of the coarse grained regions (e and f) microstructure of 'c' and 'd' after annealing at 840 ^{o}C for 1 h, respectively.

Fig. 3 shows optical micrographs of spray deposited Al-Cu-Fe + Sn alloy. It clearly reveals a light gray matrix along with a distribution of the second phase, in dark gray, having the average grain size of 4-5 µm (Fig. 3a). The white phase delineating the grain boundaries of the matrix grains was identified as the β-Sn. It is interesting to note that the Sn phase mostly delineated the boundaries of the dark gray phase. The black areas are pores. Fig. 3b shows the structure in etched condition. The white Sn phase from the boundaries has been etched out leaving black regions on the boundaries. The grains in the matrix, in light gray, are clearly revealed. The size of the grains varied in the range of 5-25 µm. The details of the phases present in the microstructure are given in Table 1. Figs. 3c and 3d show the microstructures of the material after holding at 750 °C for 2 h and 840 °C for 1h, respectively. Fig. 2c clearly reveals that the Sn phase underwent slight globularisation and the dark gray phase formed a network. Similarly, Fig. 3d reveals that the areas of the Sn phase had coalesced to each other and formed elongated networks, indicating again the flow of Sn through the grain boundaries.
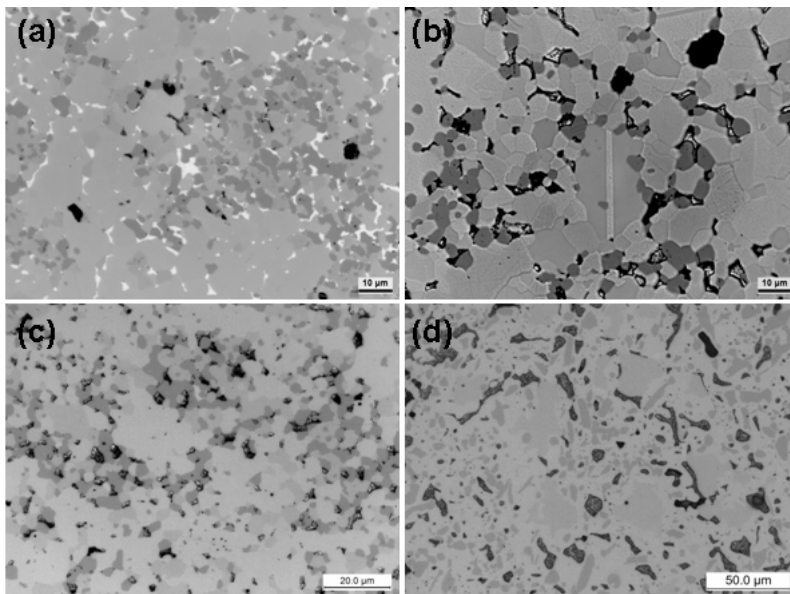

Fig. 3: Optical micrographs of the spray formed $Al_{62.5}Cu_{25}Fe_{12.5}$+Sn (a and b) microstructure containing quasicrystalline, λ- and β-phases, 'b' in etched condition (c and d) microstructure of 'a' after annealing at 750 °C for 2h and 840 °C for 1h, respectively.

X-ray element mapping and EDX analysis

The elemental X-ray mapping of the samples was carried out to ascertain the distribution of elements in the microstructures. The EDX point analysis was carried out to estimate the composition of different phases. Fig. 4 shows the elemental maps for the Al-Cu-Fe alloy in the regions of small grain size (Fig. 2a and 2c), indicating a uniform elemental distribution of Al, Cu and Fe (Figs. 4b, c and d, respectively). Although the backscattered image in Fig. 4a shows a contrast between different grains, the elemental distribution is essentially homogeneous. The composition of different grains is similar and corresponds, on an average, to 59.2 at.% Al, 28.9 at.% Cu and 11.8 at.% Fe (Table 1). Fig. 5 shows the elemental maps for Al-Cu-Fe alloy, in the region containing both coarse and fine grains as shown in Fig. 2d. Again, the elemental distribution is similar and uniform both in the small and large grains. The composition of the minor (white) phase in Figs. 5b and 5d has been identified as $Al_{13}Fe_4$ (Table 1). These are the same small (black) precipitates depicted in the optical micrograph in Fig. 2d. Fig. 6 shows the elemental maps for the Al-Cu-Fe+Sn alloy. In the backscattered image in Fig. 6a, four different phases can be detected, such as those seen in dark gray (the matrix), light gray, white and in black contrast. The black contrast originates both from the pores as well as intermetallic phase. The area with dark gray contrast has uniform distribution of elements and its composition is very similar to that observed for the matrix phase in Al-Cu-Fe

alloy, i.e. 59.0 at.% Al, 28.9 at.% Cu and 12.0 at.% Fe (Table 1). The black areas have been identified to have a composition close to the $Al_{13}Fe_4$. However, there are some pores also in the black contrast. The white areas at the grain boundaries are identified as Sn (Table 1). Despite low solubility of Al, Cu and Fe in Sn, the presence of a large amount of these elements in Sn may be due to the small particle size which leads to gathering of information from surrounding phases but may also be due to the spray forming process, as discussed later. The light gray areas have been identified to have a composition of $Al_{4.47}Cu_4Fe$, which corresponds to the β-phase. In all areas, the distribution of crystalline phases in the i-phase matrix was homogeneous.
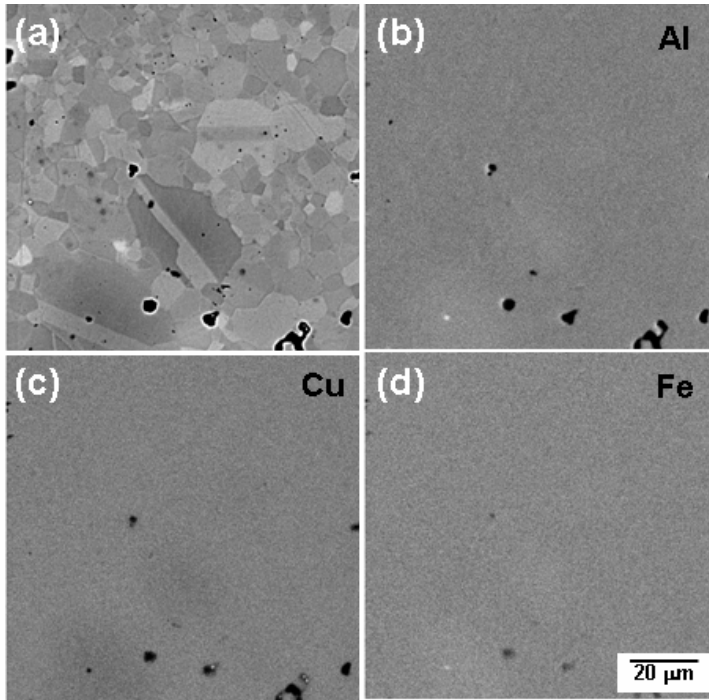

Fig. 4: (a) Back scattered image (BSI) of fine grained region in spray formed $Al_{62.5}Cu_{25}Fe_{12.5}$ (b to d) x-ray images of Al, Cu and Fe, respectively, showing a homogeneous elemental distribution
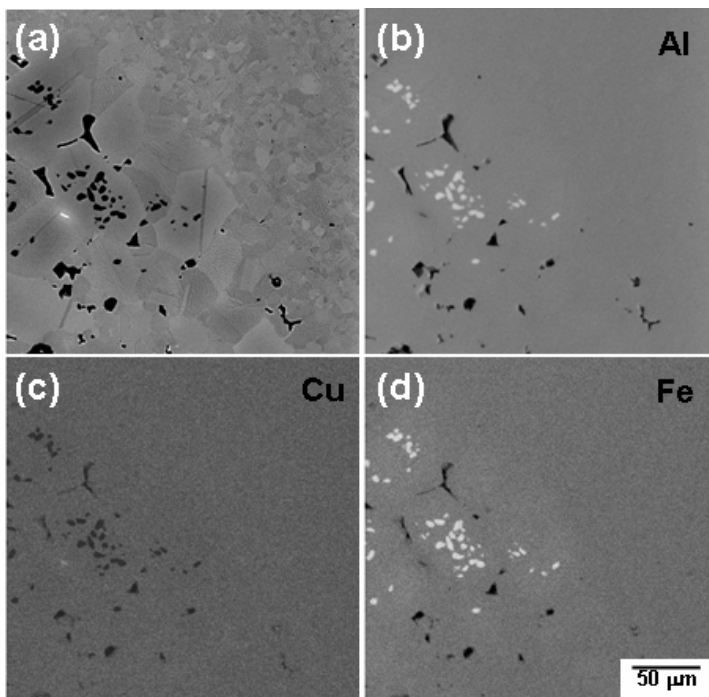

Fig. 5: (a) Back scattered image (BSI) of spray formed $Al_{62.5}Cu_{25}Fe_{12.5}$ containing coarse grains (b to d) x-ray images of Al, Cu and Fe, respectively, showing a homogeneous elemental distribution in fine grain region and λ-$Al_{13}Fe_4$ phase within coarse grains.
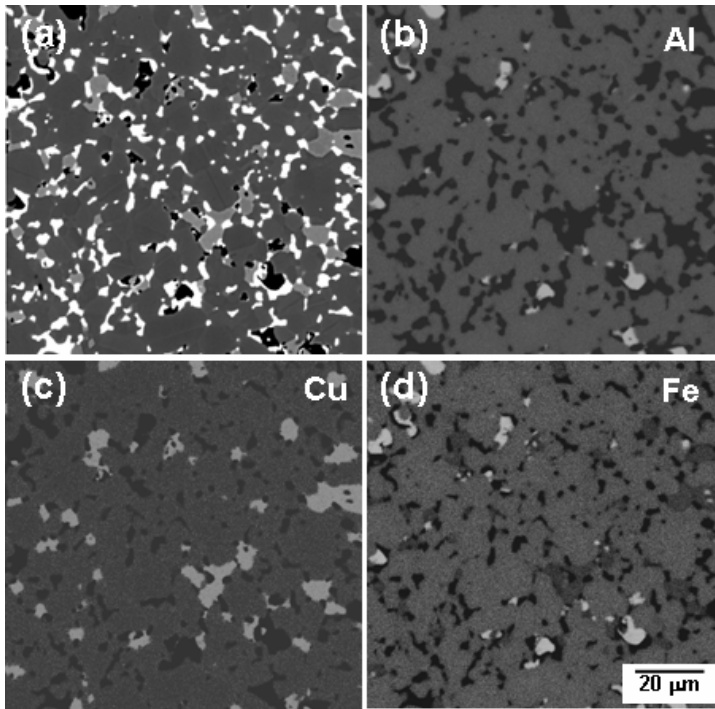
6

Fig. 6: (a) Back scattered image (BSI) of spray formed $Al_{62.5}Cu_{25}Fe_{12.5}$+Sn (b to d) x-ray images of Al, Cu and Fe, respectively, showing a homogeneous elemental distribution in the matrix and λ- and β-phases at the grain boundaries.

Transmission electron microscopy

For a more detailed microstructural characterisation, the spray-deposited Al-Cu-Fe alloy was examined by TEM, primarily to confirm the presence of the quasicrystalline phase. TEM studies revealed that the specimen was homogeneous and consisted of slightly longitudinal grains, the diameter of which varied from about 50 nm to several hundreds of nm (Fig. 7a).
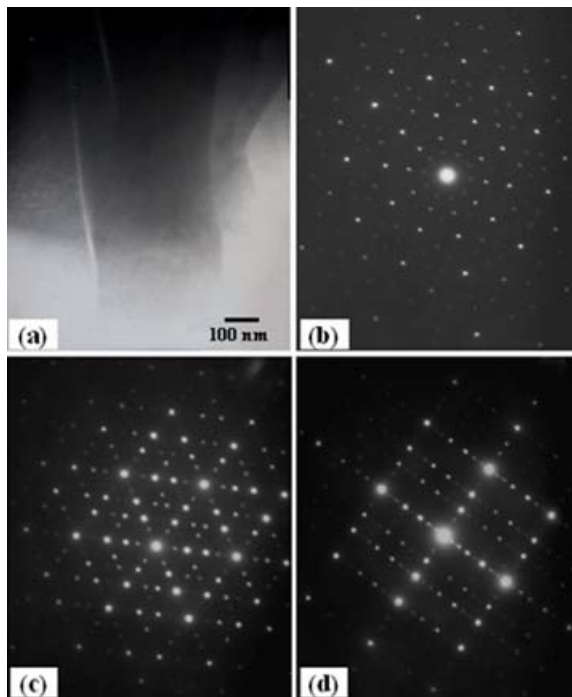

Fig. 7: (a) TEM bright field photograph showing morphology of the icosahedral phase in Al-Cu-Fe alloy and (b-d) electron diffraction patterns showing icosahedral symmetry b) SADP of fivefold axis. c) SADP of threefold axis. d) SADP of pseudo-twofold axis.

Moreover, TEM examination revealed that all grains exhibited an icosahedral symmetry, electron diffraction patterns of which are presented in Figs. 7 (b-d). When compared to the results obtained from optical microscopy and elemental mapping in SEM, it is evident that

the grains involved in the TEM specimens are small grains that form most of the Al-Cu-Fe alloy. The fact that larger grains or the $Al_{13}Fe_4$ phase were not detected by TEM analyses is reasoned by the method of specimen preparation: the section of fractured billets were first crushed in a mortar and then brought into TEM using a thin grid. Only the smallest particles were contained within the grid. The specimen preparation technique also explains why TEM examination was only conducted for Al-Cu-Fe alloy but not for Al-Cu-Fe+Sn alloy: Al-Cu-Fe+Sn was too ductile to be crushed into fine powder.

3.2 X-ray diffraction Analysis

The X-ray diffraction patterns for over-sprayed powders as well as the deposited billets are shown in Figs. 8a to 8e. The patterns for powder size -400, -350+400 and -150+350 mesh size are shown in Figs. 8a, b and c, respectively. The patterns for spray-deposits of Al-Cu-Fe and Al-Cu-Fe+Sn alloys are shown in Figs. 8d and 8e, respectively. The results clearly indicate that the peak intensity for the λ-$Al_{13}Fe_4$ and θ-Al_2Cu phases decreased with decrease in average powder size. The smallest particles of -400 mesh size contained only the β-phase along with quasicrystalline icosahedral phase (i-phase). However, the spray-formed Al-Cu-Fe alloy included only the i-phase. In contrast to Al-Cu-Fe alloy, the Al-Cu-Fe+Sn alloy was composed of the β-phase along with the i-phase and the β-Sn phase. Yet, the peak intensity of the β-phase was smaller as compared to that observed in the smallest over-sprayed powder particles. Therefore, it can be concluded that the spray-formed Al-Cu-Fe alloy introduces a single-phase icosahedral quasicrystalline structure, whereas the Al-Cu-Fe+Sn alloy contains several crystalline phases along with the i-phase.
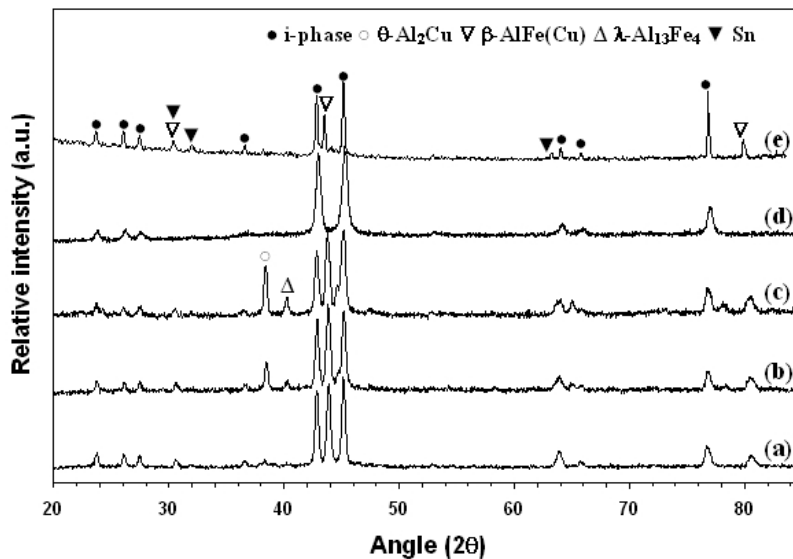

Fig. 8: X-ray diffraction patterns of (a-c) over-spray powder less than 400 mesh size (b) powder +350-400 mesh size (c) powder +150-350 mesh size (d) $Al_{62.5}Cu_{25}Fe_{12.5}$ deposit (e) $Al_{62.5}Cu_{25}Fe_{12.5}$+Sn deposit.

3.3 DSC Analysis

Figure 9 shows the DSC curves of the spray-deposited alloys. The curve for the Al-Cu-Fe alloy (Fig. 9a) reveals presence of the λ-$Al_{13}Fe_4$ and the i-phases, with the melting temperature of i-phase being 885.5°C. The curve for the Al-Cu-Fe+Sn alloy indicates five phases: the β-Sn phase (the melting temperature of which is 230°C), the θ-Al_2Cu phase (591°C), the λ-$Al_{13}Fe_4$ phase (803°C), the i-phase (833°C) and the β-AlFe phase (974°C). These results are well in agreement with those obtained by microscopy and X-ray diffractometry used in the present study.
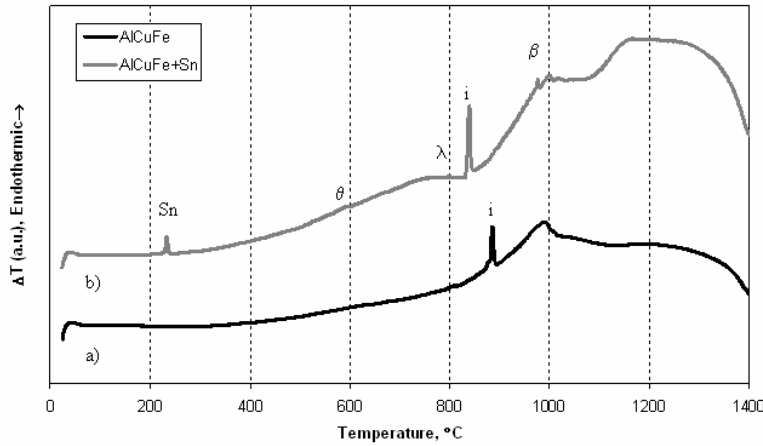
Fig. 9: DSC curves of the spray formed alloys (a) $Al_{62.5}Cu_{25}Fe_{12.5}$ deposit (b) $Al_{62.5}Cu_{25}Fe_{12.5}$+Sn deposit.

3.4 Hardness measurement

The hardness values at different indentation loads for the two alloys are shown in Fig. 10. The hardness values of 10.4 and 9.3 GPa were obtained for Al-Cu-Fe and Al-Cu-Fe+Sn alloys at an indentation load of 50 g, respectively. The hardness of Al-Cu-Fe alloy decreased with increase in indentation load, however, the rate of decrease was low after 100 g. This is known as indentation size effect [Muk06] and can be attributed to the elastic recovery effects of QC materials. The change in the hardness of Al-Cu-Fe+Sn alloy was more prominent than for the Al-Cu-Fe alloy. However, hardness became constant at the loads greater than 50 g, in contrast to Al-Cu-Fe alloy. It is emphasized that, at the load of 50 g, the indentation size was around 9.8 μm which indicates that indentation could occur within a single grain of the i-phase, thus high hardness values. However, the indentation size was around 17 μm for a load of 100 g, making it possible that the hardness value was affected by the softer phases surrounding the quasicrystalline phase.
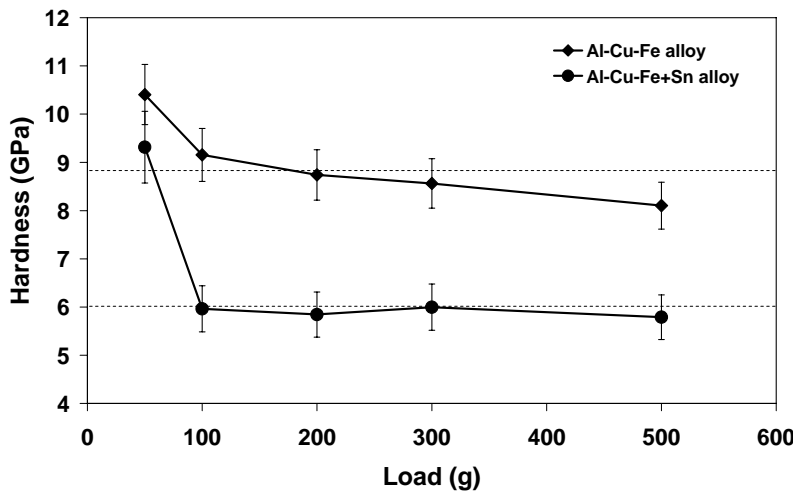

Fig. 10: Hardness values of spray deposited $Al_{62.5}Cu_{25}Fe_{12.5}$ and $Al_{62.5}Cu_{25}Fe_{12.5}$+Sn at different indentation loads.

The decreasing hardness values in the case of Al-Cu-Fe alloy may be attributed mainly to the elastic recovery effect and the smaller extent to the crack formation at the tip of the indentation, which increases with increase in load and results in increase in the indentation size. The variation of the crack length with the indentation load is given in the authors' previous paper [Sri08]. Figs. 11a and 11b show the indentation cracks at the loads of 100 and 500 g for Al-Cu-Fe alloy, respectively, revealing large intergranular cracks. In contrast, Al-Cu-

Fe+Sn alloy did not form such intergranular cracks on indentation. Figs. 11c and 11d show the indentations for Al-Cu-Fe+Sn alloy at loads of 50 and 300 g, respectively. It is evident from these micrographs that the crack length was smaller in the Sn containing alloy. The indentation at the boundary of a large grain (Fig. 11e) shows the prominent cracks and their inhibition by Sn particles at the grain boundary (indicated by arrows). Fig. 11f shows how the cracks generated at the tip of an indentation were inhibited and diverted by the presence of Sn particles. It was systematically observed in the Al-Cu-Fe+Sn alloy that the Sn particles did not allow extensive crack growth; such behaviour may lead to increase in the toughness of the material that was, indeed, observed in, e.g., preparation of TEM powder samples. This is also corroborated by the decreasing value of hardness in the Al-Cu-Fe alloy compared to an almost constant value for Al-Cu-Fe+Sn alloy with increasing applied load.
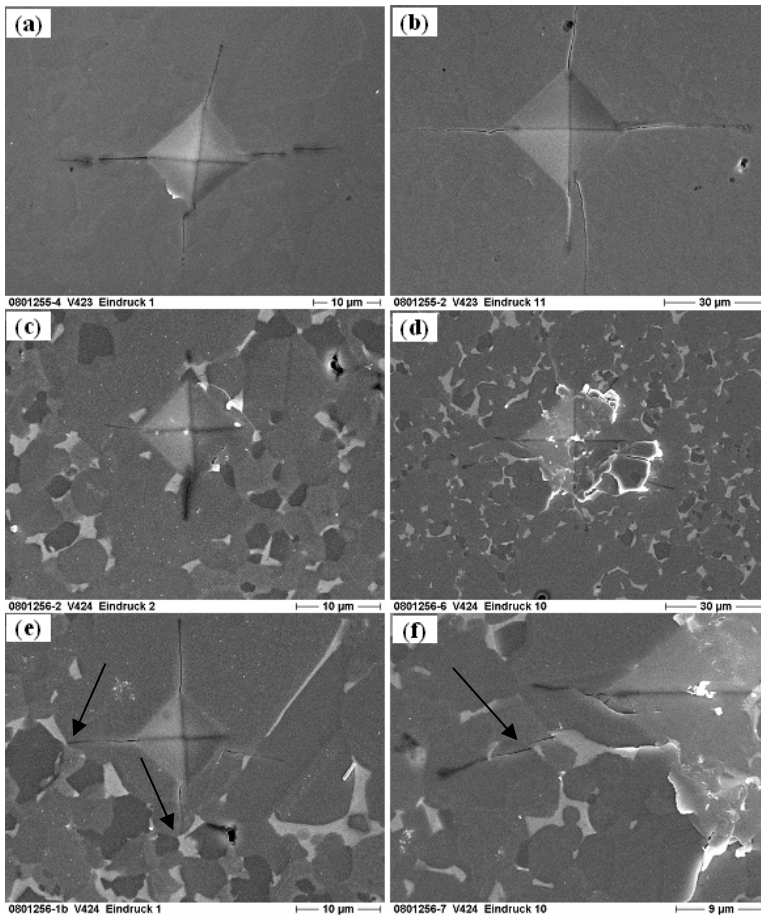

Fig. 11: SEM micrographs containing indentation marks (a and b) for 100 and 500 g load for $Al_{62.5}Cu_{25}Fe_{12.5}$ alloy, respectively (c and d) for 50 and 300 g load for $Al_{62.5}Cu_{25}Fe_{12.5}$+Sn alloy, respectively and (e and f) showing crack inhibition.

4. Discussion

The results presented in the previous sections demonstrate the efficacy of the spray forming process in the synthesis of single phase quasicrystalline material based on Al-Cu-Fe system. The microstructural evolution in the present case is of paramount importance as even the smaller size powders with high cooling rate do not show a single phase constitution. Therefore, the underlying mechanism of the formation of this microstructure is discussed in light of the process conditions prevailing during spray forming.

4.1. Spray forming process

The spray forming process consists of two distinct but integral steps: atomization of the melt into a spray of micron-size droplets and subsequent deposition of the droplets onto a

substrate. The droplets are propelled away from the atomization zone under the effect of a high-velocity gas jet and experience a cooling rate in the range 10^3-10^6 ^{o}C/s depending upon their specific surface area. The rapid solidification effect during atomization and the high-velocity impact of the droplets on the substrate or on the growing deposit gives rise to a refined and homogeneous grain structure in the deposit. However, as the deposition progresses and thickness of the deposit increases, the conductive heat transfer through the substrate decreases. A steady state condition is established when the heat transfer from the deposit takes place mainly by convective heat transfer mode under the effect of atomisation gas. A major aspect of this process lies in the fact that a large fraction of undercooled or partially solidified droplets reach the substrate. The solidification sequence of these undercooled droplets largely determines the final microstructure of the deposit. With reference to the Al-Cu-Fe system in the regime of quasicrystal forming compositions, the undercooling of droplets is supposed to play an important role, particularly considering the peritectic reaction involved with the formation of quasicrystalline phase in Al-Cu-Fe system.

4.2. Microstructural evolution

In the Al-Cu-Fe system stable quasicrystalline phase forms in the composition range of Al (54-75 at.%), Cu (21-31 at.%) and Fe (7.5-16.5 at.%) [Hut04, Ros98]. The equilibrium solidification sequence for this transformation consists of primary λ-$Al_{13}Fe_4$ phase formation in liquid that further gives rise to β-phase by a peritectic reaction and finally i-phase is formed by a second peritectic reaction. Subsequently, a metastable τ-phase forms at low temperatures. However, the solidification sequence of Al-Cu-Fe system varies with cooling rate [Lee01]. According to Faudot et al. [Fau91], single phase quasicrystalline structure is obtained in the composition range of Al (61.75-64 at.%), Cu (24-25.5 at.%) and Fe (12-12.75 at.%). There are several studies available [Hut04, Lee01, Hol97] on the solidification behaviour of Al-Cu-Fe system that include rapid solidification, conventional casting and wedge casting and magnetic levitation. However, it is evident from the reports that a clear understanding on the peritectic solidification, under non-equilibrium condition, has not yet been reached. Even then, it has been unanimously agreed that the high cooling rate and high undercooling leads to by-passing the formation of primary λ-$Al_{13}Fe_4$ phase and to suppression of the peritectic reaction. Holland-Moritz et al. [Hol97] have argued that a polytetrahedral short range order in the liquid favours the phases which are compatible with the liquid structure. They studied the $Al_{62}Cu_{25.5}Fe_{12.5}$ system by magnetic levitation and found that the degree of undercooling of icosahedral phase was lowest as compared to λ- and β-phases. Therefore, the formation of primary icosahedral phase is favoured over λ- and β-phases in highly undercooled melts. Although magnetic levitation helps in undercooling the liquid, the absence of a continuous high cooling rate may not lead to suppression of the primary λ-phase nucleation. In the spray atomisation and deposition process, however, a wide size range of droplets leads to different cooling conditions for droplets. As a result, a small droplet experiences high undercooling and therefore may witness icosahedral phase as a primary phase. Slowly cooled large droplets experience small undercooling and therefore it is highly probable that primary λ-phase nucleates and grows but, due to continuous cooling during the flight, peritectic reaction is suppressed and finally icosahedral quasicrystalline phase is formed. It is a difficult proposition, however, to quantitatively justify these arguments as the direct measurement of individual droplet's thermodynamic history is not possible. It is depicted in Figs. 2a and 2b that a major fraction of the deposit consists of fine-grained quasicrystalline phase and a minor fraction of regions containing large quasicrystal grains and small precipitates of embedded λ-$Al_{13}Fe_4$ phase. Such microstructure may be attributed to the typical distribution of droplets in the spray cone, where large droplets that experience less undercooling lie in the central region of

11

the cone. The simultaneous rotation of the inclined substrate and the scanning of the spray cone give rise to periodic deposition of large droplets on the billet. The large droplets, which experience less undercooling, contain higher heat content prior to deposition and undergo nucleation and growth of the primary λ-$Al_{13}Fe_4$ phase in the liquid. After deposition, the remaining undercooled liquid phase leads to the formation of i-phase. As the λ-$Al_{13}Fe_4$ phase is observed to be in the centre of grains, this indicates that the quasicrystalline phase forms by its deposition on the λ-$Al_{13}Fe_4$ phase by a peritectic reaction [Che07]. The high heat content of the liquid could also be inferred from the shrinkage porosity observed in the regions having large grain size. This kind of porosity is absent in the small grained regions. After annealing at 840 ^{o}C for 1 h, the λ-$Al_{13}Fe_4$ phase particles dissolve in the quasicrystalline matrix. The i-phase in $Al_{62.5}Cu_{25}Fe_{12.5}$ system shows a composition of 59.2% Al, 28.9% Cu and 11.8% Fe (at%.) as compared to 58.4% Al, 28.6% Cu and 13.0% Fe (at%.) observed by Gui et al. [Gui01]. As we see that the composition of the parent alloy and the i-phase is different, this may be indicative of some other phases present which are not detectable by XRD or SEM. On the other hand, it may be possible that there is spatial inhomogeneity in the composition of the billet. This must be seen in view of the fact that the composition of the i-phase depends on the cooling conditions and the coexisting phases that are in equilibrium with the i-phase. As the cooling conditions of the droplets in the spray cone are different, there is a possibility of spatial compositional inhomogeneity. Furthermore, the disintegration of the liquid stream in a wide size range of droplets during atomisation may lead to the division of possible impurities in only a small fraction of droplets, leaving a large fraction free of heterogeneous nucleants. This may also affect the undercoolability of the droplets, particularly in the absence of potential nucleants.

In contrast to the solidification structure of spray formed $Al_{62.5}Cu_{25}Fe_{12.5}$ system, the $Al_{62.5}Cu_{25}Fe_{12.5}$+Sn system gave rise to a different constitution of the microstructure. It has been reported that annealing of the as cast materials, atomised powder or melt spun ribbons of the Al-Cu-Fe system [Hut04, Lee01, Lee00, Ros98, Gog11] engenders single phase icosahedral quasicrystals. This has also been observed in the present study in $Al_{62.5}Cu_{25}Fe_{12.5}$ system. However, this phenomenon could not be observed in Sn containing $Al_{62.5}Cu_{25}Fe_{12.5}$ alloy. This behaviour can be speculated to be the result of (1) modification of the interfaces of the primary phases resulting in an altogether different solidification sequence. However, this aspect has not yet been reported via fundamental studies. (2) the high solid solubility of Al and Cu in liquid Sn. As the dissolution of λ- and β-phases were not observed even after annealing at 750 ^{o}C for 2 h, it can be argued that as Sn is the last phase to solidify and the alloy solidifies well above 750 ^{o}C during solidification, the dissolved Al, Cu and Fe will be rejected to the solid during last stage of Sn solidification enriching the surrounding solid phase with Al and Cu. The liquid state solubility of Fe in Sn is very low at 750 ^{o}C. It has been observed that the bulk i-phase in $Al_{62.5}Cu_{25}Fe_{12.5}$+Sn system has composition similar to that observed in $Al_{62.5}Cu_{25}Fe_{12.5}$ system. This indicates that the solidification condition may be similar in the case of $Al_{62.5}Cu_{25}Fe_{12.5}$+Sn system. However, due to the rejection of solute from Sn, the phase surrounding Sn gets enriched in Cu. Indeed, it is clearly indicated in Table 1 that the β-phase was enriched in Cu. This can also be corroborated by the fact that Sn is located at the grain boundaries and the β-phase is formed at the Sn surfaces. Furthermore, the above argument can be justified from the Fig. 3c, obtained after annealing at 750 ^{o}C for 2h, where the β-phase areas have grown together and concentrated in the areas near the Sn at grain boundaries. A further investigation is required to support this argument by annealing the material at low temperature, close to the melting temperature of Sn, for longer time.

As the deposited billet remains hot for a considerable time, an attempt was made to calculate the time-temperature profile of the billet by numerical simulation. The details of the heat transfer modelling and numerical simulation can be found in the references [Cui05,

Cui04]. The heat transfer modeling is coupled with the time-dependent geometry of the growing billet. To simplify the simulation work, the growth of the billet is assumed to be in the way of adding layers of uniform thickness one after another to the numerical grid system. Orthogonal grids are established in the cylindrical deposit for the numerical simulation. For discretization of the governing heat transfer equation an explicit finite-difference method was used. The thermal and physical properties of the materials for the deposit and the substrate are listed in Table 2. The process parameters and heat transfer parameters used for the simulation are listed in Table 3. The results of the simulation are given in Fig. 12. This shows that the temperature of the billet remains around 500-700 $^{\circ}$C for a considerable duration. This high temperature of the billet may help in dissolution of small areas of the λ- and β-phases which may be present in the slowly cooled droplets prior- or post-deposition. The complete dissolution of these phases may be expected in the small-grained regions of the billet. This assumption is made based on the fact that a wide size range of droplets is generated in the spray and complete transformation to quasicrystalline phase may be elusive.

Despite the above discussion on the possible mechanism of microstructural evolution, the authors feel that a further investigation for ascertaining the above arguments in required, which is in progress at present.
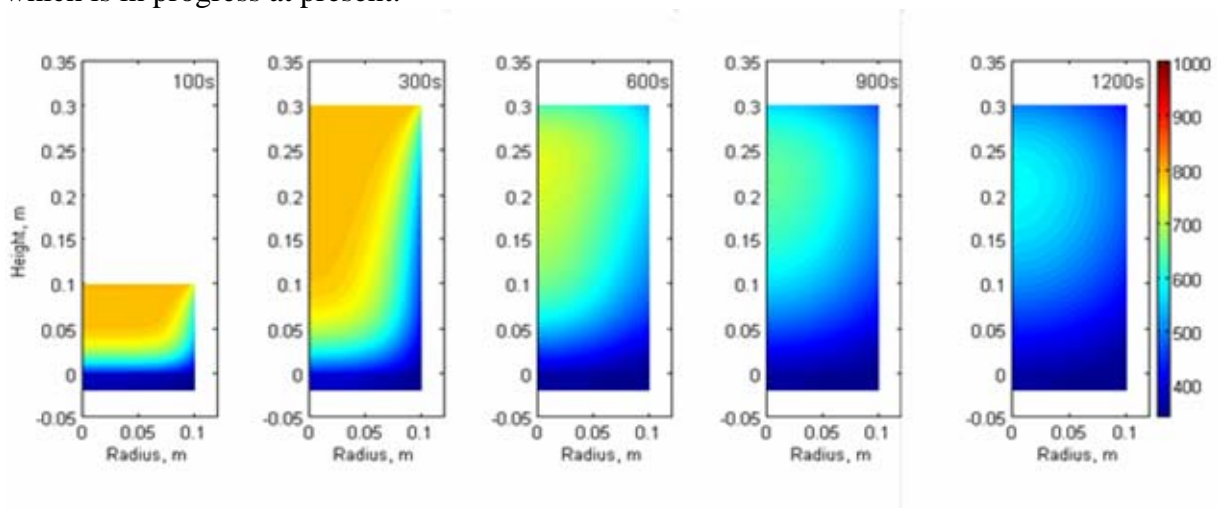

Fig. 12: Simulated time-temperature profile of the billet indicating the presence of high temperature maintained after deposition for considerable duration i.e. 900-1200 s.

7.0 Conclusions

The following conclusions could be drawn from the present study:

1) Bulk single-phase icosahedral quasicrystalline $Al_{62.5}Cu_{25}Fe_{12.5}$ could be synthesized by spray forming in a single step. The presence of Sn in $Al_{62.5}Cu_{25}Fe_{12.5}$ led to the formation of quasicrystalline phase as major phase along with minor λ- and β-phases. Even after annealing in single-phase region at 750 $^{\circ}$C for 2h, the λ- and β-phases could not be dissolved.
2) Hardness of the alloy was 10.4 GPa for $Al_{62.5}Cu_{25}Fe_{12.5}$ and and 9.3 GPa for $Al_{62.5}Cu_{25}Fe_{12.5}$+Sn at a load of 50 g. Hardness decreased due to elastic recovery effect and nucleation of indentation cracks at higher loads. A hardness value of 6 GPa was observed, for loads in the range of 100-500 g, for $Al_{62.5}Cu_{25}Fe_{12.5}$+Sn system.
3) The presence of the Sn phase restricts the crack growth and, thereby, increases the toughness of the quasicrystalline material.

4) The presence of the λ- and β-phases at the grain boundaries in the spray formed $Al_{62.5}Cu_{25}Fe_{12.5}$+Sn may be attributed to the solubility of Al, Fe and Cu in liquid Sn. Due to low melting temperature of Sn, high-temperature annealing did not introduce a single-phase quasicrystalline material.

Acknowledgements

References

[Bar01]   Barua P, Murty BS, Srinivas V, Mater Sci Eng A 304-306 (2001), 863.

[Bis05]   Biswas K, Galun R, Mordike BL, Chattopadyay K, Metall. Mater. Trans. A 36 (2005), 1947.

[Che07]   Chen YZ, Liu F, Yang GC, Liu N, Yang CL, Zhou YH, Scripta Mater. 57 (2007), 779.

[Cui04]   Cui C, Fritsching U, Schulz A, Bauckhage K, Mayr P, Mater Sci Eng A 383 (2004), 158.

[Cui05]   Cui C, Fritsching U, Schulz A, Li Q, Acta Mater. 53 (2005), 2765.

[Eck91]   Eckert J, Schultz L, Urban K, Acta Metall. Mater. 39 (1991) 1497

[Fau91]   Faudot F, Quivy A, Calvayrac Y, Gratias D, Harmelin M, Mater Sci Eng A 133 (1991), 383.

[Fle00]   Fleury E, Lee SM, Kim WT, Kim DH, J. Non-Crystalline Solids 278 (2000), 194.

[Fle04]   Fleury E, Kim YC, Kim DH, Kim DH, Kim WT, J. Non-Crystalline Solids 334-335 (2004), 449.

[Gog11]   Gogebakan M, Avar B, Tarakci M, J. Alloys and Compounds 509 (2011), S316.

[Gra95]   Grant PS, Prog Mat. Sci. 39 (1995), 497.

[Gui01]   Gui J, Wang J, Wang R, Wang D, Liu J, Chen F, J. Mater. Res. 16 (2001), 1037.

[Hol97]   Holland-Moritz D, Schroers J, Grushko B, Herlach DM, Urban K, Mater Sci Eng A 226-228 (1997), 976.

[Hut04]   Huttunen-Saarivirta E, J Alloys and Compounds 363 (2004), 150.

[Hut05]   Huttunen-Saarivirta E, Vuorinen J, Intermetallics 13 (2005), 885.

[Lee00]   Lee SM, Jung JH, Fleury E, Kim WT, Kim DH, Mater Sci Eng A 294-296 (2000), 99.

[Lee01]   Lee SM, Jeon HJ, Kim BH, Kim WT, Kim DH, Mater Sci Eng A 304-306 (2001), 871.

[Muk06]   Mukhopadhyay NK, Paufler P., Int. Mater. Rev. 51 (2006) 209

[Nic08]   Nicula R, Stir M, Turquier F, Burkel E, Mater Sci Eng A 475 (2008), 113.

[Pry02]   Pryds NH, Hattel JH, Pedersen TB, Thorborg J, Acta Mater. 50 (2002), 4075.

[Ros07]   Rosas G, Reyes-Gasga J, Pérez R, Mater Charact 58 (2007), 765.

[Ros98]   Rosas G, Perez R, Mater. Lett. 36 (1998), 229.

[Sha04]   Shao T, Cao X, Fleury E, Kim DH, Hua M, Se D, J. Non-Crystalline Solids 334-335 (2004), 466.

[Sor95]   Sordelet DJ, Kramer MJ, Unal O, J. Thermal Spray Tech. 4(3) (1995), 235.

[Sor98]   Sordelet DJ, Besser MF, Logsdon JL, Mater Sci Eng A 255 (1998), 54.
[Sri04]   Srivastava VC, Mandal RK, Ojha SN, Mater Sci Eng A 383 (2004), 14.
[Sri08]   Srivastava VC, Uhlenwinkel V, Schulz A, Zoch HW, Mukhopadhyay NK, Chowdhury SG, Z. Kristallographie 223 (2008), 711.
[Tur07]   Turquier F, Cojocaru VD, Stir M, Nicula R, Burkel E, J. Non-Crystalline Solids 353 (2007), 3417.
[Yin07]   Yin S, Bian O, Qian L, Zhang A, Mater Sci Eng A 465 (2007), 95.
[Yin08]   Yin S, Li C, Bian Q, Lu M, Mater Sci Eng A 496 (2008), 362.
[Zha02]   Zhang L, Lück R, J Alloys and Compounds 342 (2002), 53.

Table 1: Compositional analysis of different phases observed

Alloy	Location	Composition (at.%)				Possible phases
		Al	Cu	Fe	Sn	
Al-Cu-Fe	Bulk[*]	59.2	28.9	11.8	---	Icosahedral
Al-Cu-Fe	White[**]	75.2	0.6	24.2	---	λ-Al$_{13}$Fe$_4$
Al-Cu-Fe+Sn	Dark Gray[†]	59.0	28.9	12.0	0.1	Icosahedral
Al-Cu-Fe+Sn	Light Gray[†]	47.9	41.1	10.7	0.3	β-Al$_5$(Cu,Fe)$_5$
Al-Cu-Fe+Sn	White[†]	29.8	22.1	7.5	40.7	Sn
Al-Cu-Fe+Sn	Black[†]	70.4	8.4	21.1	0.1	λ-Al$_{13}$Fe$_4$

[*]See Fig. 4a; [**]See Fig. 5a; [†]See Fig. 6a

Table 2: Thermal and physical properties of the materials for the deposit and the substrate

Deposit	
Specific heat, J m^{-3} K^{-1}	488
Thermal conductivity, W m^{-1} K^{-1}	6
Liquidus temperature, K	1268
Solidus temperature, K	1123
Latent heat of fusion, J/kg	248000
Density, kg/m^3	4600
Substrate (Low carbon steel)	
Specific heat, J kg^{-3} K^{-1}	460
Thermal conductivity, W m^{-1} K^{-1}	46
Density, kg/m^3	7850

Table 3: Process parameters and heat transfer parameters used for the numerical simulation

Process parameters	
Temperature of impinging droplet, K	1173
Temperature of atomization gas, K	423
Temperature of spray chamber (inner wall), K	403
Initial temperature of substrate, K	298
Withdrawl speed of substrate, mm/s	1
Heat transfer parameters	
Convective heat transfer coefficient (deposit, top surface), W/m^{2}K	900
Convective heat transfer coefficient (deposit, side surface), W/m^{2}K	300
Convective heat transfer coefficient (substrate surface), W/m^{2}K	300
Heat transfer coefficient between deposit and substrate, W/m^{2}K	1000
Emissivity of the deposit	0.5